[2] Kreith, F. and Sonju, O. K., "The Decay of a Turbulent Swirl in a Pipe," *Journal of Fluid Mechanics*, Vol. 22, No. 2, 1965, pp.257–271.
[3] Menis, M., "Effect of Vortex Decay on Pipe Flow," Rept. 61, Nov. 1960, Gas Turbine Lab., MIT, Cambridge, Mass.
[4] Youssef, T. E. A., "Some Investigations on Rotating Flow with a Recirculation Core in Straight Pipes," Paper 66-WA-FE-36, Nov. 27, 1966, American Society of Mechanical Engineers, New York.
[5] Schlichting, H., *Boundary Layer Theory*, 4th ed., McGraw-Hill, New York, 1960, pp. 53–54.
[6] Thompson, J. R., Jr., "The Structure of Free and Confined Turbulent Vortices," Research Note 44, May 1963, Aero Physics Dept., Mississippi State University, State College, Miss.
[7] Yeh, H., "Boundary Layer Along Annular Walls in a Swirling Flow," and "Discussion," *Transactions of the ASME*, May 1958, pp. 767–776.
[8] Kinney, R. B., "Universal Velocity Similarity in Fully Turbulent Rotating Flows," ASME Paper 67-APM-23, June 1967, Applied Mechanic Conference, Pasadena, Calif.
[9] Baker, D. W., "Decay of Swirling, Turbulent Flow of Incompressible Fluids in Long Pipes," Ph.D. thesis, 1967, Univ. of Maryland, College Park, Md.
[10] Schlichting, H., *Boundary Layer Theory*, 4th ed., McGraw-Hill, New York, 1960, pp. 441–444.
[11] Schlichting, H., *Boundary Layer Theory*, 4th ed., McGraw-Hill, New York, 1960, p. 503.
[12] Schlichting, H., *Boundary Layer Theory*, 4th ed., McGraw-Hill, New York, 1960, pp. 502–508.

JULY 1974 AIAA JOURNAL VOL. 12, NO. 7

Calculation of the Flow on a Cone at High Angle of Attack

STEPHEN C. LUBARD*
R & D Associates, Santa Monica, Calif.
AND
WILLIAM S. HELLIWELL†
The Aerospace Corporation, El Segundo, Calif.

A method of predicting the flowfield on cones at high angles of attack for the supersonic laminar case is developed in this paper. An approximate system of equations obtained from the steady-state Navier-Stokes equations by assuming the viscous, streamwise derivative terms are small compared with the viscous normal and circumferential derivatives is used. These equations are valid in both the viscous and inviscid regions including the circumferential separation zone which develops on the leeward side at the higher angles of attack. A new implicit differencing technique with iteration is used to solve the resulting three-dimensional parabolic equations. This differencing scheme permits the solution to problems at the higher Reynolds numbers (10^6). Predictions are compared with experimental data for a 10° half-angle cone at 12° angle of attack at a freestream Mach number of 8 and a 5.6° half-angle cone at 8° angle of attack at a freestream Mach number of 14. Very good agreement with the data is obtained for both of these cases.

Nomenclature

Cp = specific heat at constant pressure divided by the freestream value
f = represents any of the quantities differenced
∇G^2 = $[(\partial\xi/\partial x)^2+1+(1/r\,\partial\xi/\partial\phi)^2]$
h = enthalpy divided by freestream value
j = index in the x direction
k = conductivity divided by freestream value
k = index in the η direction
L = reference length
l = index in the ϕ direction
M_∞ = freestream Mach number
M_x = local streamwise Mach number, $M_\infty u/(h)^{1/2}$
p = pressure divided by twice the freestream dynamic pressure
Pr = freestream Prandtl number
Q = heat transfer to the surface
r = metric for the ϕ coordinate; $x\sin\theta+y\cos\theta$
Re = freestream Reynolds number based on L
u = velocity in the x direction divided by freestream velocity
v = velocity in the y direction divided by freestream velocity
V_∞ = freestream velocity
w = velocity in the ϕ direction divided by freestream velocity
$\bar{x}$ = x divided by x_o
x_o = value of x where the desired angle of attack is reached
x = coordinate along the rays of the cone surface divided by L
Δx = grid spacing in the x direction
y = coordinate normal to the surface divided by L
Δy = grid spacing in the y direction
α = angle of attack
γ = ratio of specific heats
δ = increment to be added to the known iterate
η = transformed normal coordinate
$\Delta\eta$ = grid spacing in the η direction
θ = cone half angle
λ = bulk viscosity divided by freestream viscosity $(-\frac{2}{3})\mu$
μ = viscosity divided by freestream viscosity
ξ = bow shock standoff distance divided by L
ρ = density divided by freestream density
ϕ = circumferential coordinate
$\Delta\phi$ = grid spacing in the ϕ direction

Subscripts

∞ = values in the freestream
k, l = values at the given grid point, $k\to\eta$; $l\to\phi$
K = grid points at the bow shock

Presented as Paper 73-636 at the AIAA 6th Fluid and Plasma Dynamics Conference, Palm Springs, Calif., July 16–18, 1973; submitted September 5, 1973; revision received January 28, 1974. The authors would like to express their gratitude to T. Kubota of the California Institute of Technology and F. Fernandez of R & D Associates for suggesting the problem and providing many helpful suggestions during the course of the research.
Index categories: Viscous Nonboundary-Layer Flows; Supersonic and Hypersonic Flow.
* Research Scientist. Associate Member AIAA.
† Member of the Technical Staff.

Superscripts

j = values at the old x grid point
$j+1$ = values at the new x grid point
n = iteration index; known solution
$n+1$ = new iterate to be solved for

I. Introduction

THE prediction of flowfields on conical-type geometries at high angles of attack has recently received increased emphasis. This emphasis is due, in part, to the current interest in the NASA Space Shuttle. In this paper, only the circular cross-section cone will be considered, although the method which is developed can be extended to other geometries. In addition, the analytical approach will emphasize the blunted nose case at the higher laminar Reynolds numbers (10^6). Experimental data[1,2] indicate that at high angles of attack (i.e., approximately $\frac{3}{4}$ of the cone half-angle), the flow on the leeward side separates in a circumferential mode and forms two counter-rotating longitudinal vortices (Fig. 1).

Most of the previous theoretical solutions to this problem are invalid on the leeward side for angles of attack greater than that at which flow separation occurs. These theories assume a weak interaction between the viscous region and the inviscid flow. A solution to the inviscid flow is first obtained[3-5] and then a system of boundary-layer equations is used to solve for the viscous flow region.[6-8] This approach develops a singularity on the leeward side at approximately the point where flow separation occurs.[7,8]

One possible method of computing the separated flow region on a yawed cone is to apply the time-dependent techniques to solve the steady Navier-Stokes equations. The computing time and storage requirements will be extremely large if it is desired to solve the flow over the entire cone.

An alternate approach to solving the problem is developed in this paper. It is based on two important characteristics of the leeward separation (for $\alpha/\theta < 3$) which have resulted from the data of Stetson.[2] First, the separation does not occur near the tip of the cone but evolves as a rolling-up process at a distance downstream of the tip which is dependent on the nose bluntness, angle of attack, etc. Secondly, the upstream influence of the base is confined to a small region near the rear of the body (Fig. 1).

These conclusions indicate that the flow over a sharp or blunted cone (except for a small region near the base) can be modeled by dividing the body into two separate regions—the first, a nose region where the downstream boundary conditions are taken sufficiently far from the sonic line or tip to allow for closure. This region is amenable to the time-dependent techniques, and it is expected that solutions by this method will be available in the near future.[9] The second region begins at the end of this nose region and covers most of the cone surface. The data of Stetson[2] suggest that the gradients of the streamwise viscous force in this region are small.

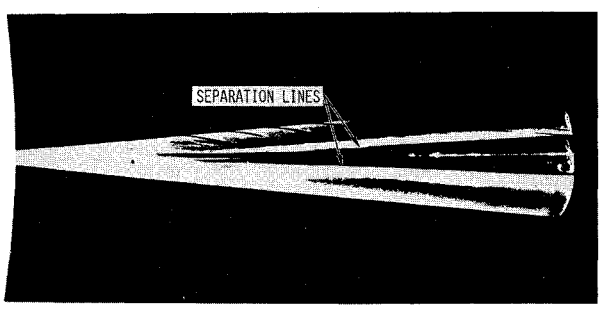

Fig. 1 An oil flow photograph of the leeward separation on a sharp 5.6° cone at 5° angle of attack (from Ref. 2).

It is the solution of the second region which comprises the major subject matter of this paper. An approximate system of equations is obtained from the steady-state Navier-Stokes equations by assuming the viscous streamwise derivative terms are small compared with the viscous normal and circumferential derivatives. A parabolic system of differential equations which is first order in x and second order in y and ϕ results. This system of partial differential equations allows a tremendous reduction in the necessary computing time and storage requirements over that which is required for the time-dependent approaches, since it is parabolic; thus a marching-type numerical solution technique can be used.

This same idea has been used previously by Rubin and Rudman and their co-workers[10-12] and Cheng et al.[13] for several two-dimensional problems and some three-dimensional cases. These previous efforts have been concerned primarily with low Reynolds number flows such as the merged layer and sharp leading edge regions. The present effort is concerned with the solution to the higher Reynolds number cases. Lin and Rubin[14,15] also recently have applied this same method to the tip and downstream boundary layer regions of a pointed cone at angle of attack. A further discussion of these two references detailing their similarities and differences to the present paper is included in Sec. 5.

In order to solve the resulting nonlinear system of parabolic equations, a new implicit-iterate differencing is used. The normal derivatives are differenced completely implicitly, that is, at the new x station and new iterate. The circumferential derivatives are differenced at the new x station but only the central and backward term is taken at the new iterate. Newton's method of iteration is then used to solve the nonlinear algebraic equations which result from the differencing. This numerical approach is similar to that proposed and studied by Rubin and Lin[16]; however, there are several important differences. Details on the differencing together with an analysis of the convergence and stability criteria are included in the paper.

The equations are solved between the body and the bow shock. Boundary conditions at the shock and its shape are calculated by using the Rankine-Hugoniot equations and a one-sided differencing of the continuity equation. This allows the solution of problems at the higher Reynolds numbers (10^6). It is also possible to integrate through the bow shock using the same system of field equations. This would permit the solution of problems at the lower Reynolds numbers.

In order to check the validity of the theoretical approach, solutions are compared with experimental data obtained by Tracy[1] on a sharp 10° half-angle cone at $\alpha = 12°$ with a Mach number of 8 and a Reynolds number of 1.13×10^6/ft; and Stetson[2] on a sharp 5.6° half-angle cone at $\alpha = 8°$ with a Mach number of 14.2 and a Reynolds number of 0.83×10^6/ft. Initial conditions for the calculation have been obtained in the present paper by slowly increasing the angle of attack from zero to the desired value and then allowing the solution to relax. Very good agreement with the available data is obtained for both of these cases.

II. The Governing Equations

Derivation of the Equations

In this section, the approximate system of equations is presented starting with the steady Navier-Stokes equations. A body-oriented coordinate system is used, with x taken along a cone generator, y normal to the surface, and ϕ the circumferential coordinate where $\phi = 0$ represents the windward ray (Fig. 2). The approximate differential equations become

$$\frac{\partial(\rho u r)}{\partial x} + \frac{\partial(\rho v r)}{\partial y} + \frac{\partial(\rho w)}{\partial \phi} = 0 \tag{1}$$

$$\frac{\partial(\rho u^2 r)}{\partial x} + \frac{\partial(\rho u v r)}{\partial y} + \frac{\partial(\rho w u)}{\partial \phi} - \rho w^2 \sin\theta + \frac{r\,\partial p}{\partial x} = \frac{r}{Re}\left\{\frac{\partial}{\partial y}\left(\mu\frac{\partial u}{\partial y}\right) + \frac{1}{r^2}\frac{\partial}{\partial \phi}\left(\mu\frac{\partial u}{\partial \phi}\right)\right\} \tag{2}$$

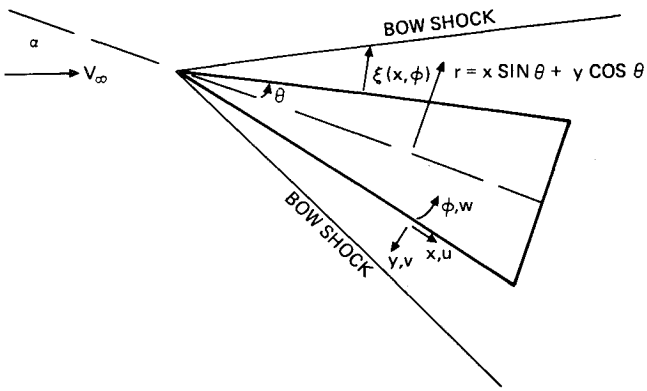

Fig. 2 Coordinate system used in the analysis.

$$\frac{\partial(\rho uvr)}{\partial x}+\frac{\partial(\rho v^2 r)}{\partial y}+\frac{\partial(\rho wv)}{\partial \phi}-\rho w^2\cos\theta+\frac{r\partial p}{\partial y}=$$
$$\frac{r}{Re}\left\{\frac{\partial}{\partial y}([\lambda+2\mu])\frac{\partial v}{\partial y}+\frac{1}{r^2}\frac{\partial}{\partial \phi}\left(\mu\frac{\partial v}{\partial \phi}\right)+\frac{1}{r}\frac{\partial}{\partial y}\left(\lambda\frac{\partial w}{\partial \phi}\right)+\frac{1}{r}\frac{\partial}{\partial \phi}\left(\mu\frac{\partial w}{\partial y}\right)\right\} \quad (3)$$

$$\frac{\partial(\rho uwr)}{\partial x}+\frac{\partial(\rho vwr)}{\partial y}+\frac{\partial(\rho w^2)}{\partial \phi}+\rho uw\sin\theta+\rho vw\cos\theta+\frac{\partial p}{\partial \phi}=$$
$$\frac{r}{Re}\left\{\frac{\partial}{\partial y}\left(\mu\frac{\partial w}{\partial y}\right)+\frac{1}{r^2}\frac{\partial}{\partial \phi}\left([\lambda+2\mu]\frac{\partial w}{\partial \phi}\right)+\frac{1}{r}\frac{\partial}{\partial y}\left(\mu\frac{\partial v}{\partial \phi}\right)+\frac{1}{r}\frac{\partial}{\partial \phi}\left(\lambda\frac{\partial v}{\partial y}\right)\right\} \quad (4)$$

$$\frac{\partial(\rho uhr)}{\partial x}+\frac{\partial(\rho vhr)}{\partial y}+\frac{\partial(\rho wh)}{\partial \phi}-r(\gamma-1)M_\infty{}^2\times$$
$$\left(u\frac{\partial p}{\partial x}+v\frac{\partial p}{\partial y}+\frac{w}{r}\frac{\partial p}{\partial \phi}\right)=\frac{r}{RePr}\left\{\frac{\partial}{\partial y}\left(\frac{k}{Cp}\frac{\partial h}{\partial y}\right)+\frac{1}{r^2}\frac{\partial}{\partial \phi}\left(\frac{k}{Cp}\frac{\partial h}{\partial \phi}\right)\right\}+\frac{(\gamma-1)M_\infty{}^2 r}{Re}\left\{\mu\left(\frac{\partial u}{\partial y}\right)^2+\frac{\mu}{r^2}\left(\frac{\partial u}{\partial \phi}\right)^2+(\lambda+2\mu)\left(\frac{\partial v}{\partial y}\right)^2+\frac{\mu}{r^2}\left(\frac{\partial v}{\partial \phi}\right)^2+\mu\left(\frac{\partial w}{\partial y}\right)^2+\frac{(\lambda+2\mu)}{r^2}\times\left(\frac{\partial w}{\partial \phi}\right)^2+2\frac{\lambda}{r}\frac{\partial v}{\partial y}\frac{\partial w}{\partial \phi}+2\frac{\mu}{r}\frac{\partial v}{\partial \phi}\frac{\partial w}{\partial y}\right\} \quad (5)$$

All the quantities appearing in Eqs. (1–5) have been nondimensionalized with the appropriate freestream quantities. Details on the derivation of these equations are included in Ref. 17. They are derived from the steady Navier-Stokes equations by assuming the derivatives with respect to x which appear in the viscous terms are of lower order compared with the derivatives with respect to both y and ϕ. In addition, $r \equiv x\sin\theta + y\cos\theta$ has been assumed to be the same order as x and therefore $\gg \partial y$ and $\partial\phi$. This will make the equations invalid for problems with very small cone angles ($\sin \ll 1$) or problems very close to the tip on a sharp cone. This restriction on r can be removed by including the additional terms in the equations which are given in Appendix A of Ref. 17.

In addition to the differential equations, an equation of state relating the density to the pressure and enthalpy and equations relating the viscosities and specific heat to the enthalpy are necessary to complete the system.

Transformation of the Normal Coordinate

For the present system, the normal boundary conditions are applied at $y = 0$ and $y \to \infty$. For the case of a very thin bow shock (high Reynolds number), jump conditions will be used and the outer boundary conditions will be taken at the bow shock. Because of the difficulty of attempting to locate the bow shock in this case, it becomes necessary to have the solution determine its location. Therefore, it is advantageous to define a new normal coordinate η such that

$$\eta = y/\xi(x,\phi) \quad (6)$$

where ξ represents the shock standoff distance normal to the body for cases where jump conditions will be used in determining the bow shock (high Reynolds number) and some a priori point in the freestream for those problems where the bow shock is integrated through (low Reynolds number).

Utilizing the transformation given in Eq. (6), the final form of differential equations is obtained. These equations become very long and are included in Appendix B of Ref. 17.

This completes the discussion of the governing field equations. These equations are parabolic in x, therefore, initial conditions at some station must be given. In addition, boundary conditions on η and ϕ must be specified.

Boundary Conditions and Initial Conditions

The boundary conditions on ϕ are reasonably straightforward. Symmetry at $\phi = 0$ (windward) and π (leeward) implies $(\partial/\partial\phi)(p, \rho, h, u, v) = 0$ and $w = (\partial^2 w/\partial\phi^2) = 0$ for all η and x.

The boundary conditions on η are more complicated. First considering the body surface ($\eta = 0$), the no-slip conditions imply $u(x, 0, \phi) = w(x, 0, \phi) = 0$ while, assuming the surface enthalpy and normal velocity are arbitrarily specified, giving v and h on the surface. The remaining quantity which must be obtained at the surface is the pressure (or density). The pressure cannot be specified a priori but is obtained as an output of the solution. The v momentum equation evaluated at the surface is used to obtain this quantity.

The outer boundary conditions, for cases where the bow shock is integrated through, are the freestream values of u, w, p, and h at $\eta = 1$. If the bow shock is thin, it is felt that integrating through the shock becomes very difficult and instead the Rankine-Hugoniot conditions are utilized to jump the shock. The jump conditions are obtained by assuming the conservation of mass, momentum, and energy across the bow shock. These conservation laws are applied in the body-oriented coordinate system.

First, the components of the freestream velocity written in the body-oriented coordinate system, become

$$\begin{aligned} u_\infty &= \cos\theta\cos\alpha - \sin\theta\sin\alpha\cos\phi \\ v_\infty &= -\sin\theta\cos\alpha - \cos\theta\sin\alpha\cos\phi \\ w_\infty &= \sin\phi\sin\alpha \end{aligned} \quad (7)$$

Next, the conservation jump conditions in the body-oriented system give

$$(u_\infty-\rho_K u_K)\frac{\partial\xi}{\partial x}-(v_\infty-\rho_K v_K)+(w_\infty-\rho_K w_K)\frac{1}{r}\frac{\partial\xi}{\partial\phi}=0 \quad (8)$$

$$\left(u_\infty\frac{\partial\xi}{\partial x}-v_\infty+\frac{w_\infty}{r}\frac{\partial\xi}{\partial\phi}\right)^2-\rho_K\left(u_K\frac{\partial\xi}{\partial x}-v_K+\frac{w_K}{r}\frac{\partial\xi}{\partial\phi}\right)^2=(\nabla G)^2(P_K-P_\infty) \quad (9)$$

$$(u_\infty-u_K)\left[\frac{1}{r^2}\left(\frac{\partial\xi}{\partial\phi}\right)^2+1\right]+(v_\infty-v_K)\frac{\partial\xi}{\partial x}-\frac{(w_\infty-w_K)}{r}\frac{\partial\xi}{\partial\phi}\frac{\partial\xi}{\partial x}=0 \quad (10)$$

$$(v_\infty-v_K)\frac{1}{r}\frac{\partial\xi}{\partial\phi}+(w_\infty-w_K)=0 \quad (11)$$

$$h_\infty+\frac{(\gamma-1)}{2}M_\infty{}^2V_\infty{}^2=h_K+\frac{(\gamma-1)}{2}M_\infty{}^2(u_K{}^2+v_K{}^2+w_K{}^2) \quad (12)$$

where the subscript K refers to the value of quantities just inside the shock at $\eta = 1$.

Equations (8–12) are five equations for the six unknowns ξ, u_K, v_K, w_K, p_K, and h_K (the equation of state relates ρ_K to p_K and h_K); therefore, an additional equation is needed. Any of the field equations which have previously been derived can be used. In this analysis, we will use the continuity equation, that is, Eq. (1) evaluated at $\eta = 1$, as the sixth equation relating the quantities at K to the interior quantities.

In addition to the required boundary conditions, initial conditions are necessary. These are to be obtained by utilizing a different solution method such as a time-dependent technique to solve the nose region up to the nose-cone tangency point. This idea permits the nose region with its possibly complicated geometry and subsonic-transonic flow to be treated separately. The solution for the nose region, including both the viscous and inviscid region at angle of attack, is not yet available. Therefore, in the present paper, initial conditions at angle of attack are generated by slowly increasing the angle of attack from zero to the desired value while marching in x and then allowing the solution to relax to the sharp-cone results.

III. Solution of the Equations

Introduction

The system of equations is parabolic in x, therefore, a marching solution technique can be utilized. A similar system of equations in Cartesian coordinates is discussed by Rubin and Lin. 16 They discuss the use of explicit, alternating direction implicit,[19] and a new "predictor-corrector" technique for solving their system. Cheng et al.[13] also discuss the solution for the Cartesian two-dimensional case at very low Reynolds number. The higher Reynolds number two-dimensional problem has been considered by Tyson[20] and Baum[21] for various geometries. These authors were interested in both relaxation and departure solutions of the equations.

Departure solutions can occur as a result of the $(\partial p/\partial x)$ term in the equations. This term permits an upstream influence to occur in the equations. Different-type solutions to the system become possible by making very small changes to the initial conditions. Some of these solutions drive to a separation-like increase in surface pressure, while others exhibit a rapid expansion-like decrease in surface pressure. As illustrated by Rubin and Lin,[16] various difference formulations for the $(\partial p/\partial x)$ terms in the equations can have a large effect on the departure solutions and also the instabilities which appear in the calculation for regions where $M_x \equiv uM_\infty/(h)^{1/2} \leqq 1$.

The following major conclusions can be obtained from Refs. 16, 20, and 21:

1) An implicit differencing, at least in the normal direction, is absolutely necessary to solve the higher Reynolds number problems.

2) Iteration to handle the nonlinear aspects of the resulting system of algebraic equations will be necessary.

3) We can expect departure solutions and instabilities because of the $(\partial p/\partial x)$ terms and the $M_x \leqq 1$ regions. Various difference formulations for $(\partial p/\partial x)$ will have to be tried to suppress these effects.

Differencing

The use of a straight implicit differencing requires the storage and inversion of very large matrices because of the three-dimensional nature of the problem under consideration. Instead, an attempt was made to use a variation of the alternating direction implicit methods.[19] It was found because of the singularity in the system at $u = 0$, near the wall, that the implicit in ϕ routine was not acceptable, although some solutions up to $\alpha/\theta = 0.8$ were obtained.

Instead, an iterative-implicit differencing is used to solve the system of equations. A similar type of differencing has been proposed and studied by Rubin and Lin.[16] Complete details of the differencing are included in Ref. 22. A brief description of the technique applied to the present system of equations is included below.

Since the equations are nonlinear, an implicit differencing results in nonlinear algebraic equations. A Newton-Raphson method is used to solve these equations, therefore the nonlinear terms are expanded in a Taylor series and terms higher than first order are dropped. It is known that this iteration procedure converges, provided the initial guess is close enough to the solution. Linearly extrapolating the solution at the previous two x stations seems to give a satisfactory initial guess. As examples of the linearization, if f^n is the known nth iterate of any variable at x^{j+1} and δf is the increment to be added to the known iterate, we have

$$\left\{r\xi\frac{\partial(\rho u)}{\partial\eta}\right\} = \left\{\left[r\xi\frac{\partial(\rho u)}{\partial\eta}\right]^n + \delta\xi\left[r\frac{\partial(\rho u)}{\partial\eta}\right]^n + \delta r\left[\xi\frac{\partial(\rho u)}{\partial n}\right]^n + (r\xi)^n\frac{\partial}{\partial\eta}(\rho^n\,\delta u + u^n\,\delta\rho)\right\} \tag{13}$$

$$\left\{\frac{\partial(\rho u)}{\partial x}\right\} = \left\{\left[\frac{\partial(\rho u)}{\partial x}\right]^n + \rho^n\frac{\delta u}{\Delta x} + u^n\frac{\delta\rho}{\Delta x}\right\} \tag{14}$$

where $\Delta x = x^{j+1} - x^j$ and the δr appearing in Eq. (13) equals $(\delta\xi)\eta\cos\theta$ since $\delta x \equiv 0$. A straight backward difference is assumed for the first derivative with respect to x terms. Therefore,

$$\left[\frac{\partial(\rho u)}{\partial x}\right]^n = \frac{(\rho u)^{j+1,n} - (\rho u)^j}{\Delta x} \tag{15}$$

The first and second derivatives with respect to ϕ and η which appear in the linearized equations are evaluated assuming unequal grid spacing in both the ϕ and η directions. Therefore, we can write

$$\frac{\partial f}{\partial\phi} = \gamma_1 f_{k,l-1} + \gamma_2 f_{k,l} + \gamma_3 f_{k,l+1}$$
$$\frac{\partial^2 f}{\partial\phi^2} = \varepsilon_1 f_{k,l-1} + \varepsilon_2 f_{k,l} + \varepsilon_3 f_{k,l+1} \tag{16}$$

A very large system of coupled linear equations for the $\delta f_{k,l}$ terms result from this differencing. In order to solve this system, a large matrix with approximately $5 \times K \times L$ rows and a band of 25 has to be inverted. Once the solution for $\delta f_{k,l}$ is obtained, it is added to $f_{k,l}^n$ to obtain a new guess for the solution at the $j+1x$ station. This procedure is Newton's method for solving nonlinear algebraic equations.

Instead of solving the full system of equations, the $\delta f_{k,l+1}$ terms are dropped and the equations are solved in the order $l = 1, 2 \ldots L$ using the boundary conditions at $l = 1$. The solution for $\delta f_{k,l}$ obtained with the $\delta f_{k,l+1}$ term neglected is added to $f_{k,l}^n$ to obtain a new guess $(f_{k,}^{n+1})$ to the solution at x^{j+1}.

The above technique uncouples the ϕ rows and, instead of having to invert a $5KL$ row matrix with a band of 25, a $5K$ row by 15 band matrix has to be inverted L times. This matrix will clearly be faster and easier to invert.

The technique which is described in the preceding paragraph is similar to the line Gauss-Seidel iteration method used to solve linear equations.[23] However, instead of solving for $\delta f_{k,l}$ exactly by iterating with $f_{k,l}^n$ held fixed, $f_{k,l}^n$ is updated after each solution is obtained. Thus we have combined a Newton's iteration method for the nonlinear equations with the Gauss-Seidel line iteration method for inverting the matrix. It should be noted that once the iterations converge, the differencing becomes completely implicit.

Convergence and Stability

The convergence and stability of the differencing scheme is addressed in detail in Ref. 22. The Newton-Raphson iteration procedure used to solve the nonlinear algebraic equations is assumed to converge. A simplified linear system of equations which only includes x and ϕ derivatives and has constant coefficients is considered. The convergence of the solution to this system of difference equations can be determined using the Fourier series method.[24] The solutions will converge if the eigenvalues of the associated amplification matrix are less than one in absolute value.

For the simplified linear system, it is found that in the region where $M_X \leqq 1$, some of the eigenvalues of the amplification matrix are always greater than one in absolute value. However, if the $(\partial p/\partial x)$ term appearing in the u momentum and static enthalpy equation is taken at the previous x step as suggested by Cheng,[13] or set equal to zero as suggested by Rubin,[16] then

convergence criteria can be obtained for $M_x < 1$. The two criteria which are obtained are

$$\Delta x < \left|\frac{ur}{w}\right| \Delta\phi \tag{17}$$

and

$$\Delta x < \frac{2|ru|\Delta\phi}{|w|[1+(1/\gamma)]+\{[1-(1/\gamma)]^2w^2+4h/\gamma M_\infty{}^2\}^{1/2}} \tag{18}$$

These results only apply to the simplified system of equations. However, it has been found from numerical experimentation on the actual nonlinear system that the results are qualitatively as predicted by Eqs. (17) and (18).

In addition to the question of convergence at a given x station, it is important to consider the stability of the difference scheme when marching in x. In performing this analysis, it is assumed that the iterations at each x station converge. The difference scheme then becomes completely implicit in the sense that all the derivatives are taken at the new station. The three variations on the $(\partial p/\partial x)$ terms, that is, differenced implicitly, at the previous x station or set identically zero, are considered.

The analysis for stability is, in reality, an attempt to delineate boundaries for obtaining relaxation as opposed to departure solutions of the system. Since we are only interested in relaxation solutions for the problem of a cone at angle of attack, and since departure solutions exhibit exponential growth, we can use the standard Fourier series analysis for stability of a linear system[24] to delineate the boundaries.

The following results are obtained from this analysis:

1) If the $(\partial p/\partial x)$ terms in the u momentum and energy equations are set equal to zero, there is no restriction on Δx for stability.

2) If the $(\partial p/\partial x)$ term is differenced at the previous x station explicity), in the u momentum and energy equations, for stability,

$$\Delta x > \frac{1}{2}\left(\frac{1}{M_x{}^2}-1\right)\frac{\rho u\, Re}{\mu\gamma}\left[1\Big/\left\{\frac{(1-\cos m_1\Delta\phi)}{r^2\Delta\phi^2}+\frac{(1-\cos m_2\Delta y)}{\Delta y^2}\right\}\right] \tag{19}$$

3) If $(\partial p/\partial x)$ is differenced implicity everywhere, Δx has to be greater than twice the right-hand side of Eq. (19). It may be recalled that an explicit differencing is required for convergence if $M_x < 1$.

Lower bound restrictions on marching step size similar to Eq. (19) have also been found for certain stiff ordinary differential equations by Curtiss and Hirschfelder[25] in order to suppress departure solutions. The case here is analogous to the ordinary differential equation case. The departure in the present case is characterized by the surface pressure oscillating or rapidly increasing and has been observed by Baum and Denison,[21] Rubin and Lin,[16] and Tyson.[20] Tyson, from numerical experiments, found that a large step size was necessary to suppress the departure solutions.

Numerical experiments with the entire system of equations agree reasonably well with Eq. (19). It should be clear that because of the upper bound restriction on Δx for convergence [Eq. (17)] and the lower bound restriction to avoid departure, a careful selection of Δx, Δy, and $\Delta\phi$ is necessary to obtain a solution.

Table 1 Parameters used in the calculations for Tracy's Case

Cone half angle	$= 10°$
Nose radius	= sharp
Freestream Reynolds number	$= 1.13*10^6$/ft
Freestream Mach number	= 8
Wall temperature/total temperature	$= 558°R/1360°R = 0.41$
Angle of attack	$= 12°$
Initial station, x_0	= 0.04 ft
Constant Prandtl number	= 0.75
Constant ratio of specific heats	= 1.4

μ calculated using Sutherland's Law

Table 2 Parameters used in the calculations for Stetson's Case

Cone half angle	$= 5.6°$
Nose radius	= sharp
Freestream Reynolds number	$= 0.83 \times 10^6$/ft
Freestream Mach number	= 14.2
Wall temperature/total temperature	= 0.8
Angle of attack	$= 8°$
Initial station, x_0	= 0.18 ft
Constant Prandtl number	= 0.75
Constant ratio of specific heats	= 1.4

μ calculated using Sutherland's Law

IV. Numerical Results

Solutions have been obtained for two cases. The first is for a sharp 10° half-angle cone at 12° angle of attack and a Mach number of 8. The freestream conditions and other necessary inputs which were used in the calculations for this example are given in Table 1. The conditions and geometry for this case have been chosen to correspond closely to the experiments performed by Tracy.[1]

The second case is a sharp 5.6° half-angle cone at 8° angle of attack and a Mach number of 14.2. The freestream conditions, etc., used in the calculations for this case are listed in Table 2. These correspond closely to the experiments performed by Stetson.[2]

Initial conditions are necessary before the solutions can be obtained. For a blunt case (which was the primary emphasis of this analysis), a solution for the nose region up to the tangency point is to be provided using time-dependent techniques. This approach is in the process of being developed.[9] For the sharp cone case, the present single-layer approach could be used to generate solutions near the tip if the terms associated with $r \to 0$ were included. This has been done by Lin and Rubin.[15] Since the primary emphasis of the present work is the blunted cone case and since the initial conditions for this problem are not as yet available, the following approach is used to generate initial conditions in order to verify the analysis and numerical approach.

Starting at zero angle of attack, initial conditions for the sharp cone case including both the viscous and inviscid regions are

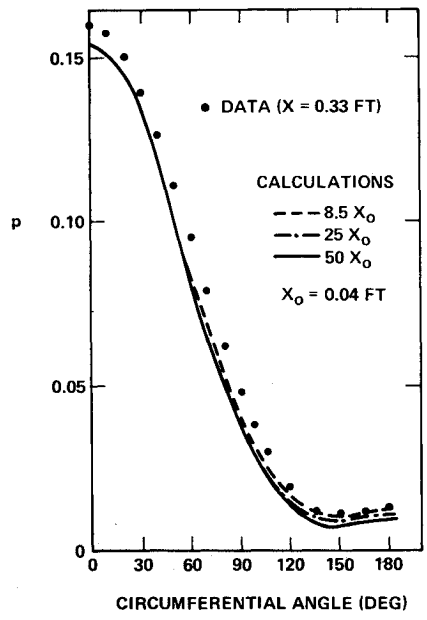

Fig. 3 Pressure distribution around the cone for Tracy's Case; $\alpha = 12°$.

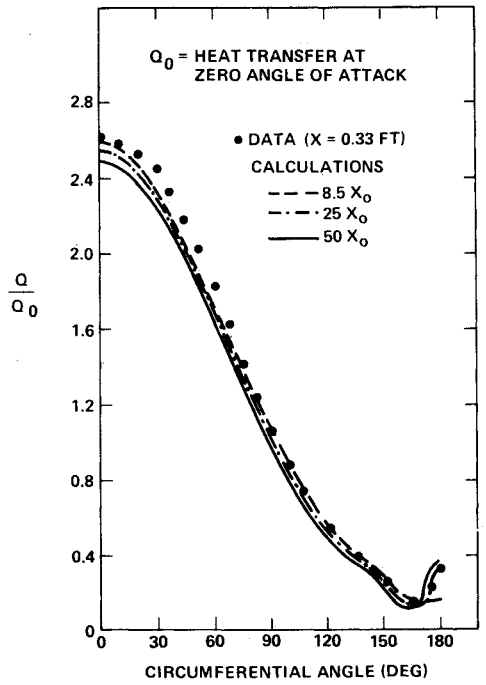

Fig. 4 Heat transfer around the cone for Tracy's Case; $\alpha = 12°$.

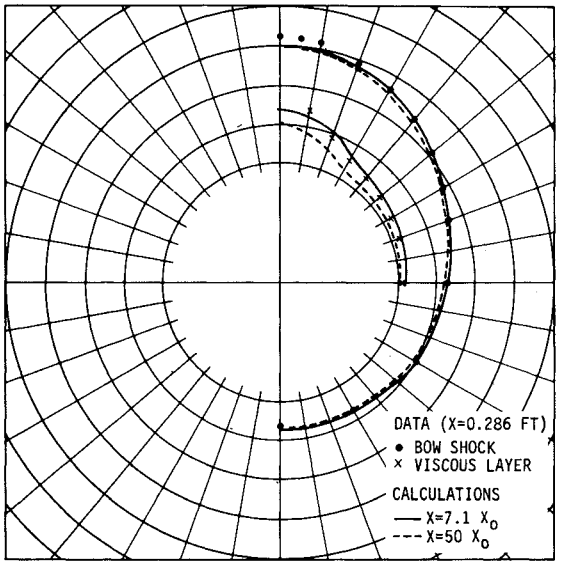

Fig. 5 Shock standoff distance and viscous layer thickness around the cone for Tracy's Case; $\alpha = 12°$.

calculated. The angle of attack is then slowly increased while marching in $x(0.5°$ per $\Delta x)$ until the desired angle of attack is reached at $x = x_o$. The calculations are then continued at a constant angle of attack and the solution is allowed to relax to the expected sharp cone results. Because of the method used to obtain the initial conditions, it is not possible to compare the results of the calculations directly with the experimental results. However, it is expected that the effect of the incorrect initial conditions will become less and less important as the solution marches downstream.

Example 1: Tracy's Case at 12° Angle of Attack

The calculated surface pressure around the cone is given in Fig. 3 for various values of $\bar{x} \equiv x/x_o$. The data measured at $x = 0.33$ ft have also been included. It appears that the pressure has reasonably well relaxed to its sharp cone value at $\bar{x} = 8.5$. Calculated results at $\bar{x} = 25$ and 50 are also given in Fig. 3 and show very little change from the results at $\bar{x} = 8.5$. The calculations are seen to be very close to the measured results with the major disagreement occurring on the windward side. This disagreement is felt to be due to the data, since Tracy[1] indicates an apparent cone angle of 10.5° for the zero angle of attack measurements. The general agreement between the shape of the data and the calculations, even though the Reynolds numbers are significantly different, indicates the surface pressure is primarily conical.

The calculated results for the heat-transfer distribution around the cone are shown in Fig. 4 for the same values of x as given for the pressure. The experimental results for $x = 0.33$ ft are also shown. The results at $\bar{x} = 8.5$ indicate that the calculations have not as yet relaxed. However, the results at $\bar{x} = 25$ and 50 show

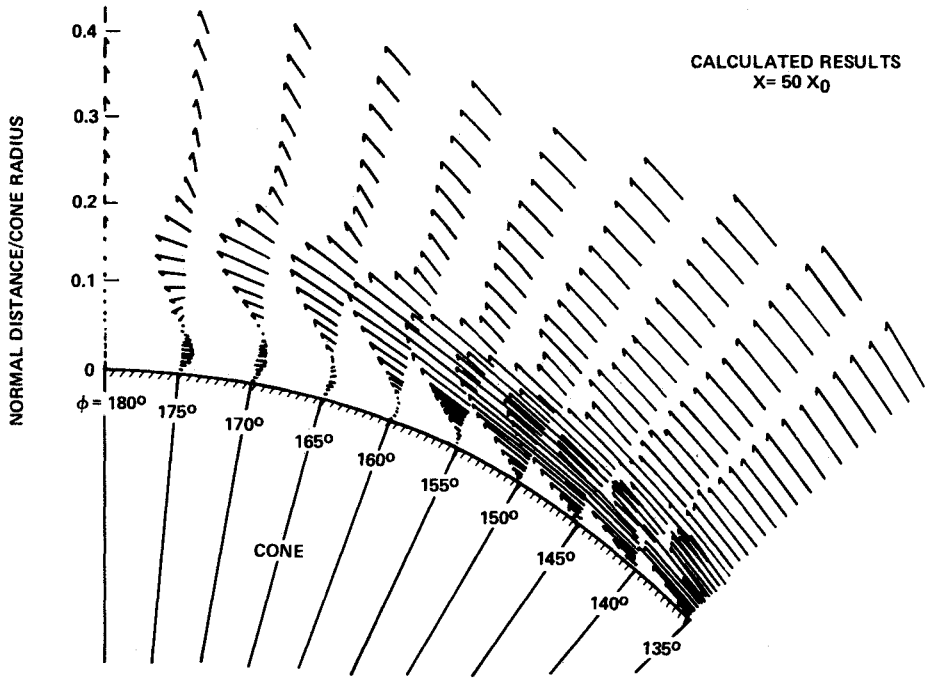

Fig. 6 Cross-plane velocity vector distribution for Tracy's Case; $\alpha = 12°$.

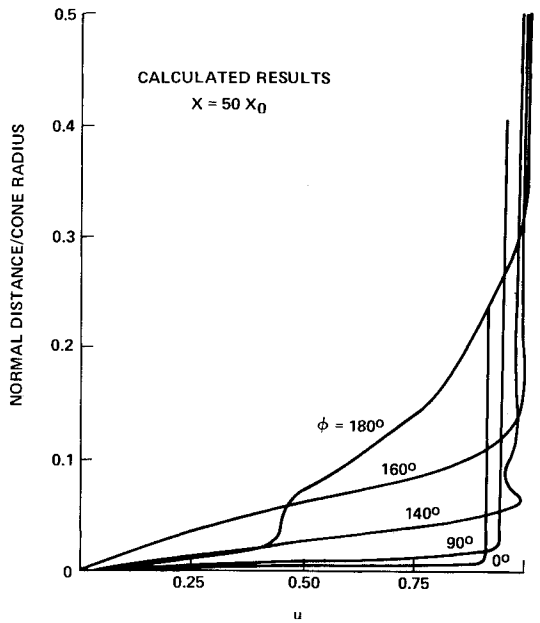

Fig. 7 Streamwise velocity profiles around the cone for Tracy's Case; $\alpha = 12°$.

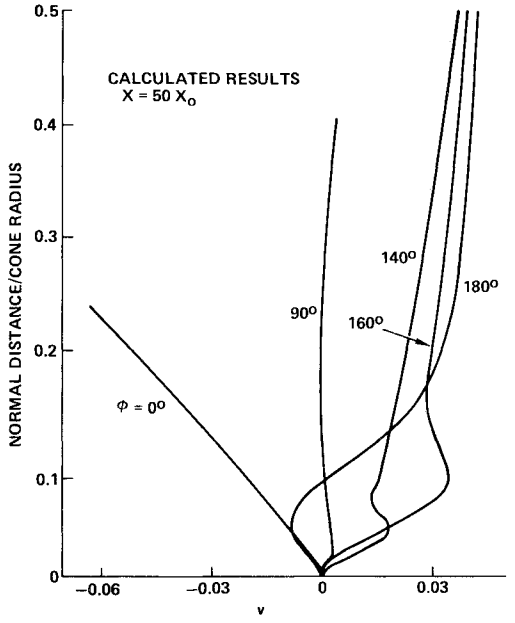

Fig. 9 Normal velocity profiles around the cone for Tracy's Case; $\alpha = 12°$.

similar trend to that given by the data and therefore are felt o be reasonably close to the sharp cone results. Both the data nd the calculations indicate a sharp increase in heat transfer rom approximately $\phi = 160°$ to $\phi = 180°$.

In Fig. 5, the calculated shock standoff distances and viscous ayer thicknesses around the cone are shown for $x = 7.1\,x_o$ 0.286 ft) and $x = 50x_o$ (2 ft). The experimental results for $= 0.286$ ft are also shown. The experimental data and the alculated results have been nondimensionalized with cone adius at the given streamwise station. The agreement between he calculated results and the data at $x = 0.286$ ft for both uantities is very good. The small disagreement on the leeside is elt to be due to the incorrect initial conditions. The calculated hock standoff distance at $x = 50x_o$ is also in good agreement with the data, indicating this quantity is primarily conical. As expected, the calculated viscous layer thickness (nondimensionalized with the local cone radius) at $x = 50x_o$ is significantly smaller than at $x = 7.1x_o$. These results indicate the incorrect initial conditions at $x = x_o$ do not significantly affect the calculation of either shock standoff distance or viscous layer thickness at $x = 7.1x_o$.

Figure 6 shows the cross-plane $(y-\phi)$ streamline distribution on the leeward side for this case at $\bar{x} = 50$. The circumferential separation bubble is clearly visible.

The calculated velocity and enthalpy profiles at $\bar{x} = 50$ for various stations around the cone are shown in Figs. 7–10. The streamwise velocity profiles (Fig. 7) and enthalpy profiles (Fig. 10) show an inflection point in the viscous region for $\phi = 180°$. This

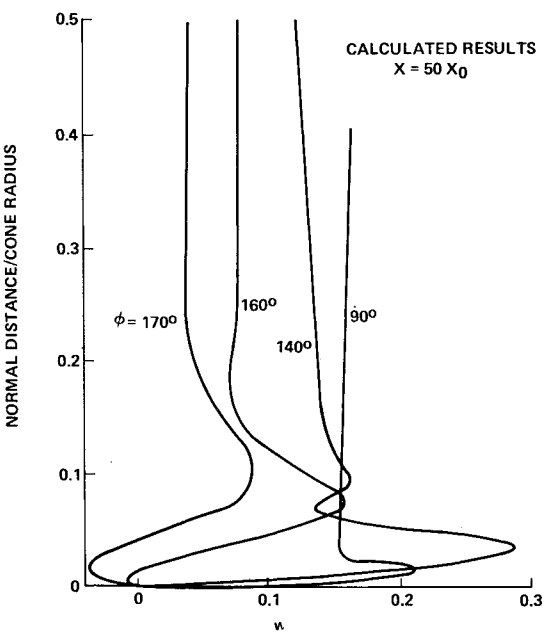

Fig. 8 Circumferential velocity profiles around the cone for Tracy's Case; $\alpha = 12°$.

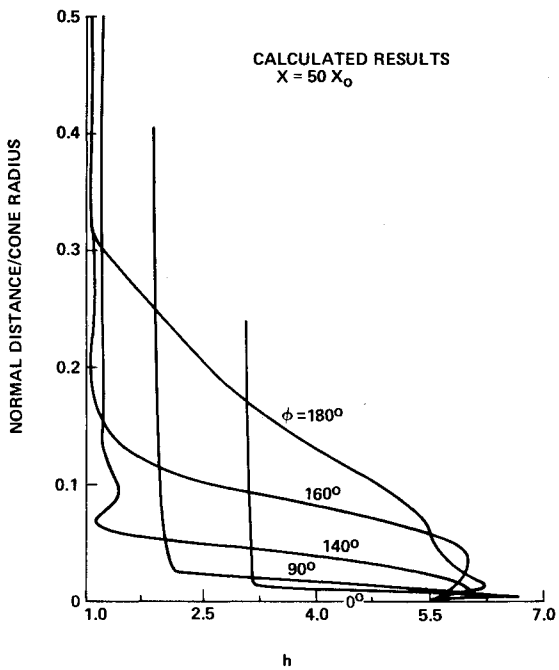

Fig. 10 Enthalpy profiles around the cone for Tracy's Case; $\alpha = 12°$.

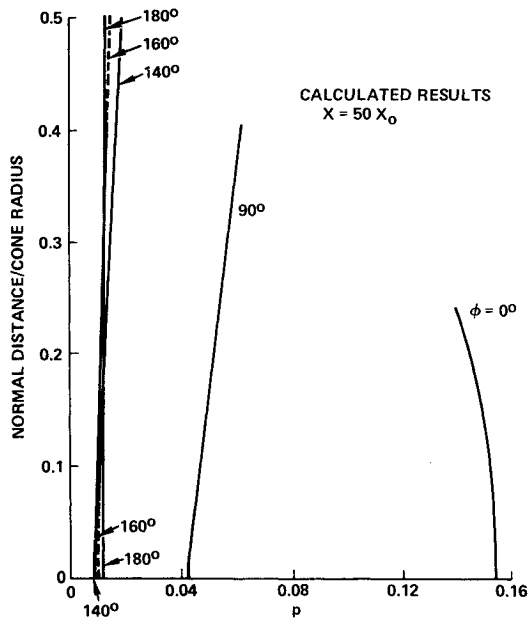

Fig. 11 Static pressure profiles around the cone for Tracy's Case; $\alpha = 12°$.

is felt to be due to the separation bubble on the leeward side. Finally, the static pressure profiles for various ϕ stations are included in Fig. 11. This case was calculated on a CDC 7600 computer and required approximately one hour to run 130 steps to $\bar{x} = 50$. The $\Delta\phi$ spacing is constant and equal to 10° and 50 unequally spaced η points were used with the $\Delta\eta$ varying from 0.0037 in the boundary layer to 0.037 in the shock layer. The required Δx from the standpoint of convergence was found to be $0.03x$. The $(\partial p/\partial x)$ terms in the u momentum and energy equations were evaluated at the previous x station for this example. Cases were also run with $(\partial p/\partial x) = 0$ and found to differ very little from those with $(\partial p/\partial x)$ explicit.

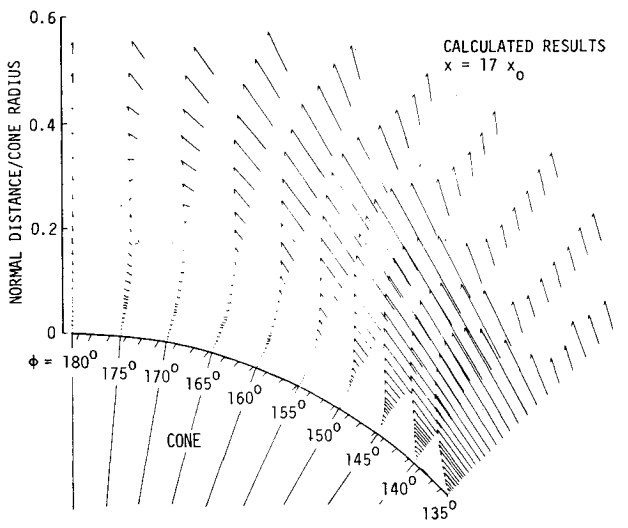

Fig. 13 Cross-plane velocity vector distribution for Stetson's Case; $\alpha = 8°$.

Example 2: Stetson's Case at 8° Angle of Attack

The freestream conditions and geometry used in the calculations for this case are given in Table 2. These are similar to those used in the experimental work of Stetson.[2] The major difference is that the surface enthalpy in the calculations is taken as constant and equal to 0.80 of the total enthalpy while the experimental data was taken with an adiabatic model. The calculated surface pressure around the cone on the leeward side for an $\bar{x} = 17$ and experimental results for $x = 0.893$ ft are shown in Fig. 12. Again there is excellent agreement, indicating the pressure is reasonably conical since the calculated results are at a significantly different Reynolds number from that of the experimental data.

The calculated results for the cross-plane streamlines are shown in Fig. 13 at $\bar{x} = 17$. Again, the circumferential separa-

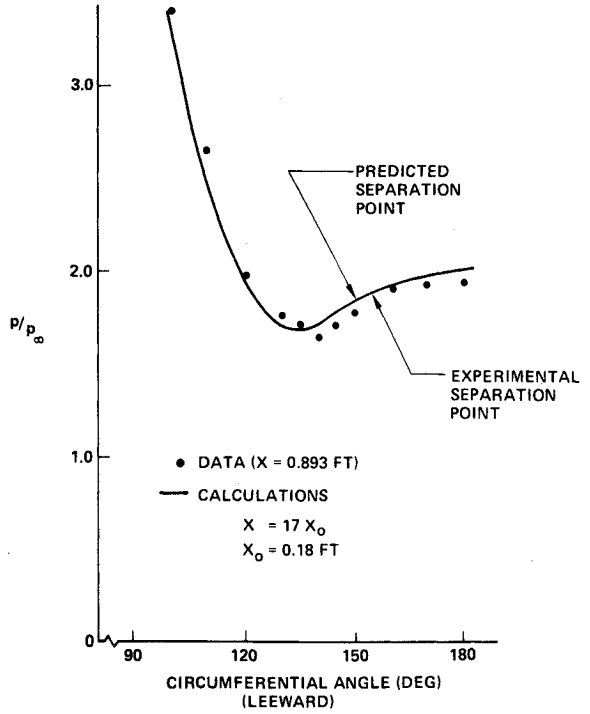

Fig. 12 Pressure distribution around the cone for Stetson's Case; $\alpha = 8°$.

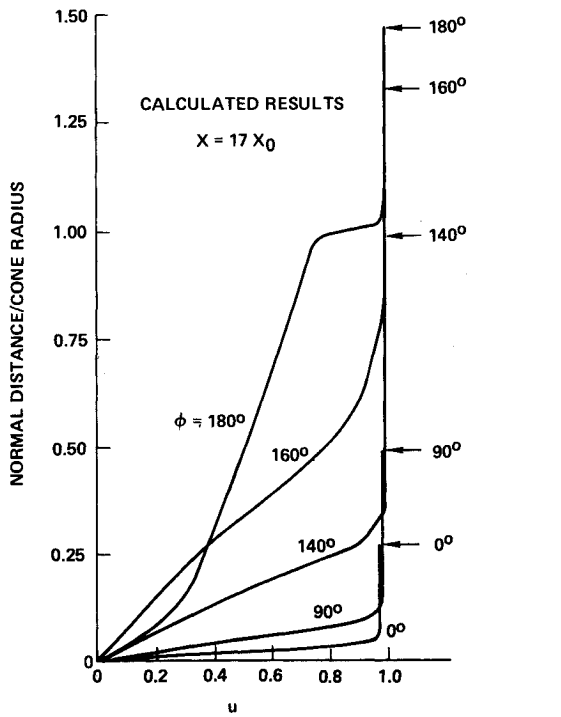

Fig. 14 Streamwise velocity profiles around the cone for Stetson's Case; $\alpha = 8°$.

tion bubble is clearly visible on the leeward side. The streamwise and circumferential velocity profiles and enthalpy profiles for several ϕ stations are shown in Figs. 14–16. The inflection point which was apparent in the previous example for the $\phi = 180°$ profiles is even more pronounced in the present example. The running time for this case for 190 steps to $\bar{x} = 17$ was approximately 90 min on the CDC 7600. The $\Delta\phi$ spacing was again constant and equal to 10°. There were 50 unequally spaced points in the η direction with the same spacing as used in Tracy's case. The $(\partial p/\partial x)$ terms in the x momentum and energy equations were set equal to zero for this case.

V. Discussion and Conclusions

A new technique for solving the flowfield on a cone at high angles of attack, including the separated region on the leeward side, has been developed. Both the viscous and inviscid regions are calculated simultaneously, and thus the interaction effects are automatically included. The approximate system of equations solved by Lin and Rubin[15] is limited to the boundary-layer region and does not allow for an interaction between the viscous and inviscid flows (except through the use of an experimentally measured surface pressure distribution). Lin and Rubin, however, were able to obtain reversed flow solutions on the leeward side for $\alpha/\theta = 2.0$. Their approach emphasizes the sharp-cone case since the initial conditions are obtained using the sharp tip merged layer solution.[14] The present analysis has been oriented to solving the blunted case where the nose region flowfield is obtained using a different solution approach.

The present analysis has also emphasized the solution to higher Reynolds number problems (10^6). This has necessitated the use of the Rankine-Hugoniot jump conditions at the bow shock instead of using the equations to integrate through the shock. It also required incorporating the calculation of the shock standoff distance directly in the equations by redefining the normal coordinate. This approach has worked extremely well.

In addition, the desire to obtain solutions at high Reynolds number requires the use of an implicit differencing technique. Because of the three-dimensional nature of the problem, a straight implicit differencing would require the inversion of exceedingly

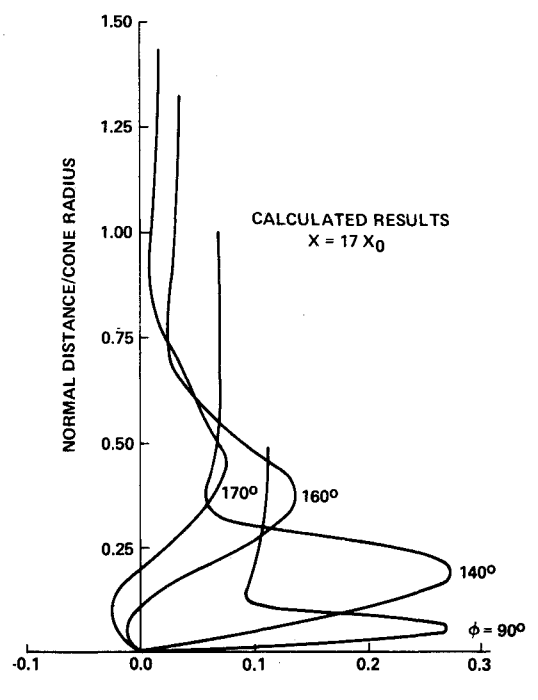

Fig. 15 Circumferential velocity profiles around the cone for Stetson's Case; $\alpha = 8°$.

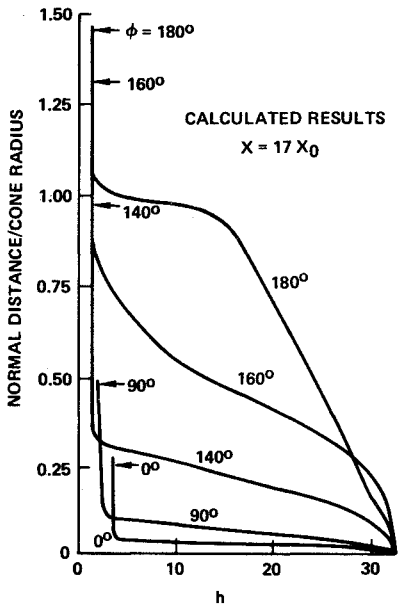

Fig. 16 Enthalpy profiles around the cone for Stetson's Case; $\alpha = 8°$.

large matrices (beyond the storage capability of the CDC 7600 computer which was used). Instead, a method similar to that proposed by Rubin and Lin[16] has been used. This method uses an iterative procedure to invert the matrices which are generated by the implicit differencing. When the iteration converges, the method becomes completely implicit. It is found there is an upper bound restriction on the Δx spacing in order to obtain convergence of the iterates.

An additional lower bound restriction on the Δx is found due to the requirement for avoiding departure solutions. This lower bound restriction is found to be a strong function of the normal spacing near the wall where reducing this spacing tends to alleviate the restriction. The required Δx is also a strong function of M_∞ and Re.

The solutions obtained using the analysis and numerical technique are found to generate the expected circumferential separation bubble on the leeward side. This separation bubble is calculated starting from an initially unseparated solution at x_o as the calculation marches downstream.

Solutions for freestream Reynolds number of 10^7 based on cone length have been generated. It is felt there would be no basic difficulties in calculating results at higher Reynolds numbers. It should also be possible to use turbulent diffusion coefficients to calculate the turbulent case. An extension of the present analysis to noncircular cones and even nonconical geometries is felt to be feasible.

References

[1] Tracy, R. R., "Hypersonic Flow Over a Yawed Circular Cone," Ph.D. thesis, Aug. 1963, Aeronautical Labs., Firestone Flight Sciences Lab., Graduate California Institute of Technology, Pasadena, Calif.

[2] Stetson, K. F., "Boundary-Layer Separation on Slender Cones at Angle of Attack," *AIAA Journal*, Vol. 10, No. 5, May 1972, pp. 642–648.

[3] Stone, A. H., "On the Supersonic Flow Past a Slightly Yawing Cone, Part II," *Journal of Mathematics and Physics*, Vol. 30, No. 4, Jan. 1952, pp. 304–312.

[4] Cook, J. C., "Supersonic Laminar Boundary Layers on Cones," TR 66347, Nov. 1966, Royal Aircraft Establishment, Farnborough, England.

[5] Moretti, G., "Inviscid Flow Field Past a Pointed Cone at an Angle of Attack," TR 577, Dec. 1965, General Applied Science Labs., Inc., Westbury, N.Y.

[6] Moore, F. K., "Laminar Boundary Layer on Cone in Supersonic Flow at Large Angle of Attack," TR 1132, 1953, NACA.

[7] Boericke, R. R., "Laminar Boundary Layer on a Cone at Incidence

in Supersonic Flow," *AIAA Journal,* Vol. 9, No. 3, March 1971, pp. 462–468.

[8] Dwyer, H. A., "Boundary Layer on a Hypersonic Sharp Cone at Small Angle of Attack," *AIAA Journal,* Vol. 9, No. 2, Feb. 1971, pp. 277–284.

[9] Victoria, K. J., "A Time Dependent Technique for Solving the Navier-Stokes Equations for an Axisymmetric Nose Tip at Angle of Attack," The Aerospace Corp., El Segundo, Calif., to be published.

[10] Rudman, S. and Rubin, S. G., "Hypersonic Viscous Flow over Slender Bodies having Sharp Leading Edges," *AIAA Journal,* Vol. 6, No. 10, Oct. 1968, pp. 1883–1889.

[11] Rubin, S. G., Lin, T. C., Pierucci, M., and Rudman, S., "Hypersonic Interactions Near Sharp Leading Edges," *AIAA Journal,* Vol. 7, No. 9, Sept. 1969, pp. 1744–1751.

[12] Cresci, R. J., Rubin, S. G., Nardo, C. T., and Lin, T. C., "Hypersonic Interaction Along a Rectangular Corner," *AIAA Journal,* Vol. 7, No. 12, Dec. 1969, pp. 2241–2246.

[13] Cheng, H. K., Chen, S. Y., Mobley, R., and Huber, C. R., "The Viscous Hypersonic Slender-Body Problem: A Numerical Approach Based on a System of Composite Equations," RM 6193-PR, May 1970, The Rand Corp., Santa Monica, Calif.

[14] Lin, T. C. and Rubin, S. G., "Viscous Flow over a Cone at Incidence, Part 1: Merged Layer," *Journal of Computers and Fluids,* Vol. 1, Jan. 1973.

[15] Lin, T. C. and Rubin, S. G., "Viscous Flow over a Cone at Incidence, Part 2: Boundary Layer," *Journal of Fluid Mechanics,* Vol. 1, July 1973, pp. 593–620.

[16] Rubin, S. G. and Lin, T. C., "Numerical Methods for Two and Three-Dimensional Viscous Flow Problems: Application to Hypersonic Leading Edge Equations," *Journal of Computational Physics,* Vol. 9, No. 2, April 1972, pp. 339–364.

[17] Lubard, S. C. and Helliwell, W. H., "Calculation of the Flow on a Cone at High Angle of Attack," RDA TR 150, Feb. 1973, R & D Associates, Santa Monica, Calif.

[18] Moretti, G., "The Choice of a Time Dependent Technique in Gas Dynamics," PIBAL Rept. 69-26, July 1969, Polytechnic Institute of Brooklyn, Brooklyn, N.Y.

[19] Douglas, J., Jr. and Gunn, G. E., "A General Formulation of Alternating Direction Methods," *Numerische Mathematik,* Vol. 6, 1964, pp. 428–453.

[20] Tyson, T. J., "Laminar Boundary Layers in the Neighborhood of Abrupt Spatial Disturbances," Ph.D. thesis, June 1957, Graduate Aeronautical Labs., California Institute of Technology, Pasadena, Calif.

[21] Baum, E. and Denison, M. R., "Interacting Supersonic Laminar Wake Calculations by a Finite Difference Method," *AIAA Journal,* Vol. 5, No. 7, July 1967, pp. 1224–1230.

[22] Helliwell, W. H. and Lubard, S. C., "An Implicit Method for Three-Dimensional Viscous Flow with Application to Cones at Angle of Attack," presented at the Symposium on Computers and Fluids, Polytechnic Institute of Brooklyn, Brooklyn, N.Y., Jan. 1973.

[23] Isaacson, E. and Keller, H. B., *Analysis of Numerical Methods,* Wiley, New York, 1966.

[24] Richtmyer, R. D. and Morton, K. W., *Difference Methods for Initial Value Problems,* 2nd ed., Interscience, New York, 1967.

[25] Curtiss, C. F. and Hirschfelder, J. O., "Integration of Stiff Equations," *Proceedings of the National Academy of Sciences,* Vol. 38, No. 3, 1952, pp. 235–243.